Thermochimica Acta 666 (2018) 156–165

Contents lists available at ScienceDirect

Thermochimica Acta

journal homepage: www.elsevier.com/locate/tca

Mn(II), Fe(II), Co(II), Ni(II), Cu(II) and Zn(II) transition metals isonicotinate complexes: Thermal behavior in N_2 and air atmospheres and spectroscopic characterization

Wilhan Donizete Gonçalves Nunes[a], José Augusto Teixeira[a], Bruno Ekawa[a], André Luiz Carneiro Soares do Nascimento[a], Massao Ionashiro[a], Flávio Junior Caires[a,b,*]

[a] Universidade Estadual Paulista (UNESP), Instituto de Química, Araraquara, SP, Brazil
[b] Universidade Estadual Paulista (UNESP), Faculdade de Ciências, Bauru, SP, Brazil

ARTICLE INFO

Keywords:
Isonicotinate
Thermal behavior
Bivalent transition metals
Pyrolysis
Evolved gas analysis

ABSTRACT

Solid-state $M(IN)_2{\cdot}nH_2O$ complexes, where M stands for bivalent transition metals (Mn, Fe, Co, Ni, Cu and Zn), IN is isonicotinate and n = 0.5 to 4.0 H_2O, were synthesized. Characterization and thermal behavior of the compounds were performed employing elemental analysis (EA), complexometric titration with EDTA, powder X-ray diffraction (PXRD), infrared spectroscopy (FTIR), simultaneous thermogravimetry and differential scanning calorimetry (TG–DSC) in dynamic dry air and nitrogen atmospheres, differential scanning calorimetry (DSC) and TG–DSC coupled to FTIR. The thermal behavior of isonicotinic acid and its sodium salt was also investigated in both atmospheres. The dehydration of these compounds occurs in a single step in both atmospheres. In air atmosphere, the thermal decomposition of the anhydrous compounds also occurs in a single step, except for the copper compound where two steps are observed. In N_2 the thermal decomposition of the anhydrous compounds occurs in two consecutive steps, except for iron compound, where three steps are observed. The main gaseous products of thermal decomposition/pyrolysis of the compounds were identified as CO, CO_2 and Pyridine. Mn, Co, Cu and Zn compounds show a physical transformation process in DSC curves. The ligand coordinates through the pyridine nitrogen atom to the metal and for the Zn compound, the carboxylate group also participates in the coordination. The IR absorption profile of hydrated and dehydrated compounds suggest that there is a probable change in the coordination mode of the ligand upon dehydration. This change needs to be further investigated, once it is not possible to ensure only with infrared spectroscopy data.

1. Introduction

A literature survey of coordination compounds with organic ligands results in a wide variety of papers describing applications for this type of material. The investigations focus mainly in synthesize and characterize functional materials for gas storage, catalysis, drug delivery, luminescent materials, molecular sieves, improved biological activity of pharmaceuticals, etc. When it comes to the ligand isonicotinate (4-pyridinecarboxilate) it is very interesting for obtaining such materials due to its ability to coordinate by two sites (pyridine nitrogen atom, and carboxylate group), forming polymeric porous materials [1–5].

The formation of complexes between bivalent transition metals and isonicotinate ligand was also already described as a possible method for gravimetric determination of these elements [6]. In such application, knowing its stoichiometry and thermal stability is crucial, once the precipitate in such method needs to be dried at elevated temperatures.

Concerning the structure of some complexes, depending on the synthetic conditions employed the isonicotinate ligand can coordinate by both the carboxylate group and pyridyl N atom (under solvothermal conditions [7]) or just by the pyridyl N atom (in aqueous solution) [8].

Besides the already mentioned applications, the study of the thermal behavior of metal complexes can lead to the identification of stable intermediates during the thermal decomposition. These intermediates can be interesting in some applications, and therefore obtaining it by thermal methods could be an alternative way for producing compound that sometimes would be difficult to obtain by other routes. Some studies described the thermal behavior of isonicotinate complexes and proposed a degradation mechanism in nitrogen atmosphere [9,10]

Although the literature on the isonicotinate coordination compounds shows a variety of approaches for the compound's characterization, there is a lack of an extensive study on the thermal behavior of isonicotinate transition metal complexes in different atmosphere

* Corresponding author at: Universidade Estadual Paulista (UNESP), Faculdade de Ciências, Bauru, SP, Brazil.
E-mail address: flavio.caires@unesp.br (F.J. Caires).

https://doi.org/10.1016/j.tca.2018.06.010
Received 16 February 2018; Received in revised form 16 June 2018; Accepted 19 June 2018
Available online 23 June 2018
0040-6031/

conditions. So, the focus of the current research was to investigate the thermal behavior (employing TG-DSC, DSC and EGA/TG-FTIR) of some bivalent transition metals isonicotinate complexes in dynamic dry air and nitrogen atmospheres to determine its minimal formula, thermal stability, and gaseous products evolved during oxidation (air) and pyrolysis (N_2). Also, a spectroscopic investigation by FTIR and PXRD were conducted to obtain structural information.

2. Experimental

Isonicotinic acid with 99% purity was obtained from Aldrich and used as received. Aqueous solution of sodium isonicotinate 0.1 mol L^{-1} was prepared by neutralization of an aqueous solution of isonicotinic acid with sodium hydroxide solution 0.1 mol L^{-1}. Aqueous 0.1 mol L^{-1} solutions of bivalent transition metal ions were prepared by dissolving the correspondent chloride [Mn(II), Co(II), Ni(II)] or sulphate [Fe(II), Cu(II), Zn(II)].

The solid-state compounds were obtained by adding slowly with stirring 100 mL of sodium isonicotinate 0.1 mol L^{-1} to 50 mL of the respective metal ions solutions 0.1 mol L^{-1} heated up to near ebullition. The system was cooled down to room temperature and the precipitates were filtered off, washed with distilled water until chloride (Cl^-) or sulphate (SO_4^{2-}) ions were eliminated (tested with $AgNO_3$/HNO_3 solution for Cl^- ions or $BaCl_2$ for SO_4^{2-} ions) dried at 50 °C in a forced circulation air oven for 12 h and kept in a desiccator over anhydrous calcium chloride. To avoid the oxidation of Fe(II) to Fe(III), all the solutions, as well as the water used for washing the precipitate, were purged with nitrogen gas, even during the heating to near ebullition and cooling to room temperature.

For the compounds in the solid state the metal, hydration water and isonicotinate contents were determined from TG curves obtained in dry air atmosphere. The metal ions content were also determined by complexometry with standard EDTA solution after calcinating the compounds in a furnace to obtain the respective oxides and dissolving in hydrochloric acid solution [11].

Carbon, hydrogen and nitrogen contents were determined by microanalytical procedures with a CHN elemental analyzer from Perkin Elmer, model 2400 and from TG curves (dry air atmosphere), since the ligand lost in the thermal decomposition occurs with the formation of the respective oxides with known stoichiometry as final residue.

Simultaneous TG–DSC curves were obtained in a Mettler Toledo thermal analysis system, model TG–DSC 1. As purge gas, dynamic dry air or nitrogen (99% purity), with a flow rate of 50 ml min^{-1} in both cases, were used. When nitrogen atmosphere was employed, the system was purged for 20 min before starting the analysis. The heating rate was set as 10 °C min^{-1}, with samples weighting about 10 mg. As sample support, 150 µL alumina (α–Al_2O_3) crucibles were used.

The evolved gas analysis (EGA/TG–FTIR) experiments were performed coupling the thermogravimetric analyzer to the Nicolet FTIR spectrophotometer equipped with a gas cell, using DTGS detector with KBr window. The furnace outlet was couplet to the heated (at 250 °C) spectrophotometer gas cell were coupled through a heated (at 225 °C) 120 cm stainless steel transfer line with diameter of 3 mm, both purged dry air and N_2 (50 mL min^{-1}). The FTIR spectra were recorded with 16 scans per spectrum at a resolution of 4 cm^{-1}.

The DSC experiments were performed in a TA Instruments model Q10 differential scanning calorimeter. Dry air or nitrogen was employed as purge gas, both at a flow rate of 50 mL min^{-1}. The heating rate of 10 °C min^{-1} and sample mass of about 2 mg were adopted. Aluminum crucible with perforated cover was used as sample support.

The attenuated total reflectance (ATR) infrared spectra for the compounds were run in a Nicolet iS10 FTIR spectrophotometer, using an ATR accessory with Ge window. The spectrophotometer was equipped with a DTGS detector. Each spectrum was acquired with 32 scans and resolution set to 4 cm^{-1}.

The powder X-ray diffractograms (PXRD) were obtained using a Siemens X-ray diffractometer, model D-5000, employing CuKα radiation (λ = 1.541 Å), operating voltage of 40 kV, current of 20 mA. Glass sample supports were used, and the samples were exposed to the radiation with incidence angles (2θ) swept from 5º to 80º, at a step of 0,02º with collection time of 2 s.

3. Results and discussion

3.1. TG-DSC of isonicotinic acid and sodium isonicotinate

The TG–DSC curves of isonicotinic acid (HIN) in dynamic dry air and nitrogen atmospheres are shown in Fig. 1. In both conditions, the TG–DSC curves show total mass loss in a single step between 165–260 °C, attributed to sublimation of the compound. It was confirmed by heating the isonicotinic acid in a glass tube up to 260 °C. A white solid, deposited on the glass wall, were collected, and by IR analysis it was identified as isonicotinic acid.

For sodium isonicotinate (NaIN), the TG–DSC curves in air and N_2 atmospheres are also shown in Fig. 1. These curves show mass losses in three consecutive steps, in both atmospheres, with thermal events

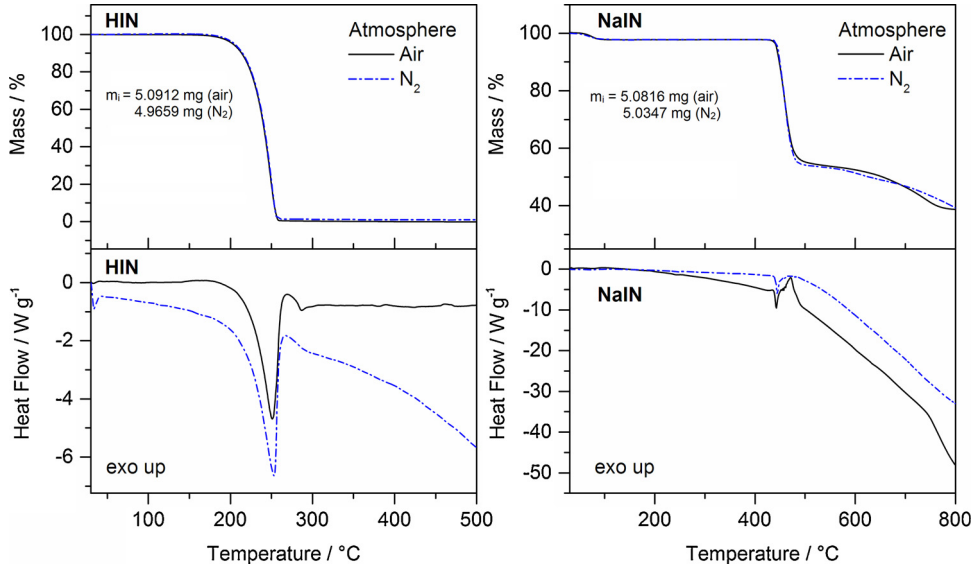

Fig. 1. Isonicotinic acid (HIN) and sodium isonicotinate (NaIN) TG–DSC curves in air and N_2 atmospheres.

corresponding to these losses, even though in some cases thermal events cannot be observed. The first mass loss between 50–95 °C (air, N_2) with mass loss of 2.45% and 2.29%, respectively, is attributed to dehydration with loss of 0.2 H_2O ($\Delta m_{calcd.}$ = 2.42%). No thermal event corresponding to the dehydration is observed in the TG curve in both atmospheres. This is attributed to the fact that the dehydration occurs so slowly that a low heat flow rate is involved in this step, therefore it does not produce a noticeable thermal event.

The anhydrous compound is stable up to 430 °C in both atmospheres. Above this temperature the thermal decomposition (air) or pyrolysis (N_2) occur in two consecutive steps between 430–530 °C and 530–790 °C (air) or 430–520 °C and 520 – > 1000 °C (N_2). In the first step the endo and exothermic peaks at 445 °C and 470 °C (air) or endothermic peaks at 450 and 460 °C (N_2), with mass loss of 43.62% (air) and 44.32% (N_2) are attributed to the thermal decomposition and oxidation of the organic matter and/or of the gaseous products evolved during thermal decomposition (air) and pyrolysis (N_2) with formation of sodium carbonate and carbonaceous residue (air) and carbonaceous residue (N_2). The last step with mass loss of 15.37% (air) and 22.40% with mass loss still being observed (N_2) is attributed to oxidation and pyrolysis of the carbonaceous residue, respectively. In the last step, no thermal event is also observed, probably because it occurs slowly, and the heat involved is not sufficient to produce thermal event, as mentioned for the first step (dehydration).

3.2. Analytical results for isonicotinate metal complexes

For the synthesized compounds the analytical and thermoanalytical (TG) results are presented in Table 1. From these results the stoichiometry of the compounds was established, which agree with the general formula $M(IN)_2{\cdot}nH_2O$, where M stands for bivalent transition metals, IN is isonicotinate and n = 3 (Mn), 3.5 (Fe, Cu) and 4 (Co, Ni, Zn).

3.3. TG-DSC of isonicotinate metal complexes

Simultaneous TG–DSC curves in dynamic dry air and N_2 atmospheres for the synthesized compounds are shown in Fig. 2a–f, and a*–f*, respectively. These curves show mass losses in two or three steps (air), and three or four steps (N_2), and thermal events corresponding to these losses or due to physical phenomenon.

From these curves it was possible to conclude that the thermal stability of the hydrated compounds (I) depends only on the nature of the metal ion. Differently, the stability of the anhydrous compounds (II) and the final temperature of thermal decomposition (III) depend on the nature of the metal ion and of the purge gas used:

I) Air and N_2: Ni (125 °C) > Co (110 °C) > Fe (100 °C) > Cu (90 °C) > Mn (80 °C) > Zn (40 °C).
II) Air: Co = Zn (365 °C) > Mn (340 °C) > Ni (305 °C) > Cu = Fe (260 °C).

N_2: Mn (380 °C) > Co (370 °C) > Zn (365 °C) > Ni (295 °C) > Fe = Cu (255 °C).

(III) Air: Zn (460 °C) > Mn (450 °C) > Co (430 °C) > Ni (410 °C) > Fe (400 °C) > Cu (375 °C).

N_2: Mn (> 1000 °C) > Zn (900 °C) > Ni (890 °C) > Cu (810 °C) > Co (765 °C) > Fe (720 °C).

As the thermal behavior of the compounds depends on the nature of the metal ion and atmosphere used, the features of each compound are discussed individually and for each atmosphere separately.

3.3.1. TG–DSC in air atmosphere

3.3.1.1. Manganese compound. The simultaneous TG–DSC curves for manganese compound are shown in Fig. 2a. The first mass loss between 80 and 190 °C, corresponding to an endothermic peak at 120 °C is due to dehydration with loss of 3 H_2O ($\Delta m_{calcd.}$ = 15.30%; Δm_{TG} = 15.26%). The anhydrous compound is stable up to 340 °C and above this temperature the thermal decomposition occurs in a single step between 340 and 450 °C with mass loss of 63.43%, corresponding to a large exothermic peak attributed to oxidation of the organic matter and/or of the gaseous products evolved during the thermal decomposition, with the formation of Mn_3O_4 as final residue. The small mass gain (Δm_{TG} = 0.48%), between 450 and 470 °C is attributed to partial oxidation reaction of Mn_3O_4 to Mn_2O_3 and the mass loss between 910 and 930 °C (Δm_{TG} = 0.82%) corresponding to an endothermic peak at 915 °C is attributed to the reduction reaction of Mn_2O_3 to Mn_3O_4 [12]. The endothermic peak at 250 °C without mass loss in the TG curve is attributed to phase transition process and is further discussed in the PXRD section.

3.3.1.2. Iron compound. The simultaneous TG–DSC curves for iron compound are shown in Fig. 2b. These curves show mass losses in two consecutive steps (TG) although the DSC curve suggests that the second step occurs through two overlapping ones. The first mass loss between 100 and 160 °C, corresponding to an endothermic peak at 145 °C is attributed to dehydration with loss of 3.5 H_2O ($\Delta m_{calcd.}$ = 17.37%; Δm_{TG} = 17.35%). The anhydrous compound is stable up to 260 °C and above this temperature the thermal decomposition occurs between 260 and 400 °C with loss of 60.73%, corresponding to exothermic peaks at 365 and 390 °C attributed to oxidation of Fe(II) to Fe(III) and oxidation of the organic matter and/or of the gaseous products evolved during the thermal decomposition with formation of Fe_2O_3 as final residue ($\Delta m_{calcd.}$ = 78.01%; Δm_{TG} = 78.08%).

3.3.1.3. Cobalt compound. The simultaneous TG–DSC curves for cobalt compound are shown in Fig. 2c. These curves show mass losses in three steps and thermal events corresponding to these losses or due to physical phenomenon. The first mass loss between 110 and 174 °C, corresponding to an endothermic peak at 155 °C is attributed to dehydration with loss of 4 H_2O ($\Delta m_{calcd.}$ = 19.21%; Δm_{TG} = 19.36%). The anhydrous compound is stable up to 365 °C and above this temperature the thermal decomposition occurs in a single step between 365 and 430 °C, with loss 59.35%, corresponding to a large

Table 1
Analytical and thermoanalytical (TG*) data for $M(IN)_2{\cdot}nH_2O$ compounds.

Compounds	Metal oxide/%			IN (Lost)/%		Water/%		C/%			N/%			H/%			Final Residue
	Calcd.	EDTA	TG	Calcd.	TG	Calcd.	TG	Calcd.	EA	TG	Calcd.	EA	TG	Calcd.	EA	TG	
$Mn(IN)_2{\cdot}3H_2O$	21.59	21.41	21.79	63.11	62.95	15.30	15.26	40.80	41.25	40.70	7.96	8.55	7.94	4.00	3.48	3.99	Mn_3O_4
$Fe(IN)_2{\cdot}3.5H_2O$	21.99	22.41	21.92	60.64	60.73	17.37	17.35	39.69	39.12	39.73	7.72	7.30	7.73	4.17	4.25	4.17	Fe_2O_3
$Co(IN)_2{\cdot}4H_2O$	21.39	21.60	21.29	59.40	59.35	19.21	19.36	38.41	38.85	38.46	7.49	7.35	7.50	4.31	4.50	4.32	Co_3O_4
$Ni(IN)_2{\cdot}4H_2O$	19.90	20.15	20.05	60.88	60.58	19.22	19.37	38.43	38.71	38.37	7.47	7.80	7.46	4.31	4.02	4.30	NiO
$Cu(IN)_2{\cdot}3.5H_2O$	21.45	21.82	21.41	61.54	61.37	17.01	17.22	38.86	38.72	38.88	7.56	7.85	7.56	4.04	3.73	4.09	CuO
$Zn(IN)_2{\cdot}0.5H_2O$	25.54	25.28	25.78	71.63	71.21	2.83	3.01	45.24	44.82	45.09	8.79	9.11	8.76	2.85	2.71	2.84	ZnO

* TG in air atmosphere; IN = isonicotinate; M = bivalent transition metal.

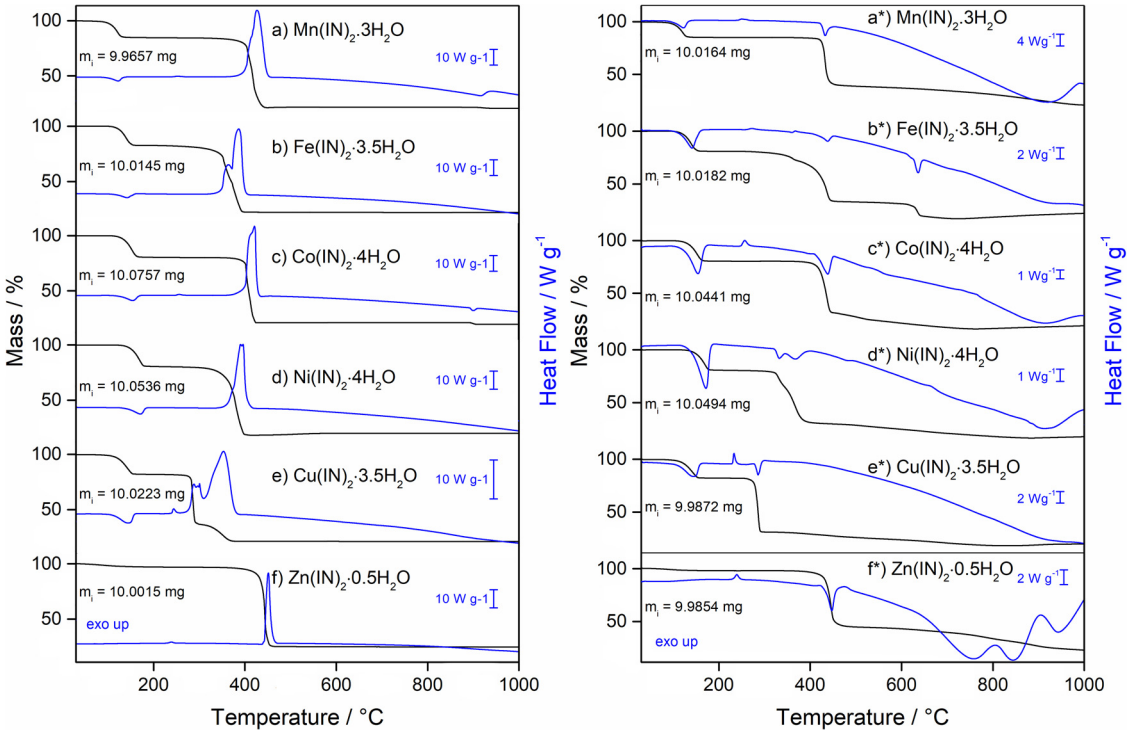

Fig. 2. TG–DSC curves of the synthesized metal complexes in air (a–f) and N_2 (a*–f*) atmospheres.

exothermic peak at 425 °C attributed to oxidation of the organic matter and/or of the gaseous products evolved during the thermal decomposition. The total mass loss up to 430 °C agrees with the formation of Co_3O_4 as final residue ($\Delta m_{calcd.}$ = 78.61%; Δm_{TG} = 78.71%). The last mass loss of 1.39%, between 890 and 910 °C corresponding to an endothermic peak at 900 °C, is due to reduction of Co_3O_4 to CoO and in agreement with the literature [12]. The exothermic peak at 260 °C, without mass loss in the TG curve is attributed to phase transition.

3.3.1.4. Nickel compound. The simultaneous TG–DSC curves for nickel compound are shown in Fig. 2d. The first mass loss between 125–185 °C corresponding to an endothermic peak at 170 °C is attributed to dehydration with loss of 4 H_2O ($\Delta m_{calcd.}$ = 19.22%; Δm_{TG} = 19.37%). The anhydrous compound is stable up to 305 °C and above this temperature the thermal decomposition occurs in a single step between 305 and 410 °C, with loss of 63%, corresponding to an exotherm with two peaks at 390 and 400 °C attributed to oxidation of the organic matter and/or the gaseous products evolved during the thermal decomposition with the formation of a mixture of Ni° to NiO. At higher temperatures there is oxidation of Ni° to NiO, and the mass loss up to 800 °C agrees with the formation of NiO as final residue ($\Delta m_{calcd.}$ = 80.10%; Δm_{TG} = 79.95%).

3.3.1.5. Copper compound. The simultaneous TG–DSC curves for copper compound are shown in Fig. 2e. These curves show mass losses in three consecutive steps and thermal events corresponding to these losses or due to physical phenomenon. The first mass loss between 90 and 160 °C, corresponding to an endothermic peak at 145 °C is due to dehydration with loss of 3.5 H_2O ($\Delta m_{calcd.}$ = 17.01%; Δm_{TG} = 17.22%). The anhydrous compound is stable up to 260 °C and above this temperature the thermal decomposition occurs in two consecutive steps between 260–375 °C, with losses of 46.03% and 15.34%, corresponding to an exothermic peak at 350 °C, respectively, attributed to the oxidation of organic matter and/or of the gaseous products evolved during the thermal decomposition. The total mass loss up to 375 °C agrees with the formation of CuO as final residue ($\Delta m_{calcd.}$ = 78.55%; Δm_{TG} = 78.59%). The exothermic peak at 245 °C, without mass loss in the TG curve is attributed to phase transition.

3.3.1.6. Zinc compound. The simultaneous TG–DSC curves for zinc compound are shown in Fig. 2f. The first mass loss between 40 and 140 °C, without thermal event in the DSC curve is attributed to dehydration with loss of 0.5 H_2O ($\Delta m_{calcd.}$ = 2.83%; Δm_{TG} = 3.01%). No thermal event due to dehydration is observed, probably because the small mass loss occurs slowly, and the heat involved is not sufficient to produce the endothermic peak. The anhydrous compound is stable up to 365 °C and between 365–460 °C the thermal decomposition occurs in a single step with loss of 71.21%, corresponding to a large and sharp exothermic peak at 450 °C attributed to the oxidation of organic matter and/or of the gaseous products evolved during the thermal decomposition. The total mass loss up to 460 °C agrees with the formation of zinc oxide, ZnO, as final residue ($\Delta m_{calcd.}$ = 74.46%; Δm_{TG} = 74.22%). The small exothermic peak at 240 °C, without mass loss in the TG curve is attributed to phase transition process.

3.3.2. TG–DSC in N_2 atmosphere

The TG–DSC curves in N_2 atmospheres are shown in Fig. 2a*–f*. These curves show mass losses in three steps, (except for iron compound where four steps are observed) and endothermic peaks attributed to dehydration and thermal decomposition, exothermic peak attributed to physical phenomenon or without thermal event. A thermal decomposition mechanism was proposed for each compound based on mass losses and the gaseous evolved products identified by TG coupled to FTIR (see next section).

3.3.2.1. Manganese compound. The TG–DSC curves of the compound are shown in Fig. 2a*. These curves show mass losses in three consecutive steps, with mass loss still being observed up to 1000 °C. the first mass loss between 75 and 140 °C corresponding to an endothermic peak at 125 °C is attributed to dehydration with loss of 3 H_2O ($\Delta m_{calcd.}$ = 15.30% (Eq. (1a)); Δm_{TG} = 14.68%).

The anhydrous compound is stable up to 380 °C and above this temperature the mass losses occur in two consecutive steps of loss mass

between 380–1000 °C. The first step between 280 – 460 °C (fast process), corresponding to the endothermic peak at 435 °C, is attributed to the thermal decomposition of the compound leading to the formation of Mn_2O_3 and carbonized residue, with release of CO_2, pyridine (C_5H_5N) (both identified by EGA), N_2 and H_2 (not detectable by IR), according to the Eq. (1b) ($\Delta m_{calcd.}$ = 47.05% (Eq. (1b)), Δm_{TG} = 45.04%).

The last step of mass loss between 460 – > 990 °C is attributed to the slow oxidation of the carbonized material formed in the previous step ($\Delta m_{calcd.}$ = 19.83% (Eq. (1c)), Δm_{TG} = 18.88%). The total mass loss up to 1000 °C suggests the formation of MnO and a small amount of remaining carbonaceous material ($\Delta m_{calcd.}$ MnO = 79.91%, $\Delta m_{calcd.}$ MnO + 0.75C = 77.37%); Δm_{TG} = 78.60%), as final residue, with release of CO.

$$Mn(IN)_2{\cdot}3H_2O\ (s) \longrightarrow Mn(IN)_2\ (s) + 3H_2O\ (g) \quad (1a)$$

$$4Mn(IN)_2\ (s) \longrightarrow 2Mn_2O_3(s) + 5CO_2(g) + 5C_5H_5N(g) + 13C(s) + 3/2N_2(g) + 7/2H_2(g) \quad (1b)$$

$$2Mn_2O_3(s) + 13C(s) + 4O_2(g)^* \longrightarrow 4\,MnO(s) + 3C(s) + 10CO(g) \quad (1c)$$

*Residual O_2 in the N_2 purge gas

3.3.2.2. Iron compound. The TG–DSC curves of the compound are shown in Fig. 2b*. These curves show mass losses in four steps between 100 and 720 °C and mass gain between 720 – > 1000 °C. The first mass loss between 100 and 160 °C, corresponding to an endothermic peak at 140 °C is attributed to dehydration with loss of 3.5 H_2O ($\Delta m_{calcd.}$ = 17.37% (Eq. (2a)); Δm_{TG} = 17.60%).

The anhydrous compound is stable up to 255 °C and above this temperature the mass losses occur in three consecutive steps, being the first two overlapping ones, between 55–370 °C (Δm_{TG} = 8.57%) and 370–455 °C (Δm_{TG} = 38.80%), corresponding to endothermic peaks at 360 °C and 440 °C. These two steps suggest a decomposition mechanism with release of CO_2, (C_5H_5N) (both identified by EGA), N_2 and H_2 (not detectable in IR) ($\Delta m_{calcd..}$ = 49.89% (Eq. (2b)), Δm_{TG} = 47.37%) resulting in the formation of Fe_2O_3 and carbonized organic matter, as evidenced by visual inspection and PXRD of the sample heated to 455 °C (see Fig. S1 in supplementary material), and is in disagreement with that reported in the literature [13].

The third mass loss step between 455–720 °C, associated with the endothermic peak at 640 °C, is attributed to the oxidation-reduction reaction between the iron oxide and the carbonized material with formation of Fe° and CO. ($\Delta m_{calcd.}$ = 15.43 (Eq. (2c)), Δm_{TG} = 16.50%). The total mass loss up to 720 °C agrees with the formation of Fe° and a small amount of C ($\Delta m_{calcd.}$ Fe° = 84.62%, $\Delta m_{calcd.}$ Fe° + 1.25C = 80.49% (Eq. (2c)), Δm_{TG} = 82.78%). The mass gain above 720 °C up to 1000 °C is attributed to oxidation of the Fe° to FeO ($\Delta m_{calcd.}$ = 4.41% (Eq. (2d)), Δm_{TG} = 5.05%) [14,15].

$$Fe(IN)_2{\cdot}3.5H_2O(s) \longrightarrow Fe(IN)_2(s) + 3.5H_2O(g) \quad (2a)$$

$$4Fe(IN)_2(s) \longrightarrow 2Fe_2O_3(s) + 13C(s) + 5CO_2(g) + 6C_5H_5N(g) + N_2(g) + H_2(g) \quad (2b)$$

$$2Fe_2O_3(s) + 13C(s) + O_2(g)^* \longrightarrow 4Fe^\circ(s) + 5C(s) + 8CO(g) \quad (2c)$$

$$2Fe^\circ(s) + O_2(g)^* \longrightarrow 2FeO(s) \quad (2d)$$

*Residual O_2 in the N_2 purge gas.

3.3.2.3. Cobalt compound. The TG–DSC curves of the compound are shown in Fig. 2c*. The first mass loss between 105 and 175 °C, corresponding to an endothermic peak at 155 °C is attributed to dehydration with loss of 4 H_2O ($\Delta m_{calcd.}$ = 19.21% (Eq. (3a)); Δm_{TG} = 19.29%).

The anhydrous compound is stable up to 370 °C and above this temperature the mass losses occur in two consecutive steps between 370–765 °C. The first step of mass loss between 370–450, associated to the endothermic peak at 440 °C in the DSC curve, is attributed to the thermal decomposition of the compound, with release of CO_2, (C_5H_5N) (both identified by EGA), N_2 and H_2 (not detectable in IR), leading to the formation of CoO and carbonized material ($\Delta m_{calcd.}$ = 51.22% (Eq. (3b)), Δm_{TG} = 48.66%). The second step of mass loss, without thermal events in the DSC curve, is attributed to the slow oxidation-reduction reaction between CoO and carbonized material with the formation of Co^0 and CO ($\Delta m_{calcd.}$ = 14.93% (Eq. (3c)), Δm_{TG} = 15.49%). The total mass loss up to 765 °C, suggest the formation of a mixture of Co^0 and carbonaceous residue ($\Delta m_{calcd.}$ Co^0 = 84.29%, $\Delta m_{calcd.}$ Co + 1.5C = 79.49%, Δm_{TG} = 83.45%). The mass gain observed between 765–1000 °C is attributed to the oxidation of the Co^0 to CoO ($\Delta m_{Calcd.}$ = 4.26% (Eq. (3d)), Δm_{TG} = 3.07%) [14,15].

$$Co(IN)_2{\cdot}4H_2O(s) \longrightarrow Co(IN)_2(s) + 4\,H_2O(g) \quad (3a)$$

$$4\,Co(IN)_2\ (s) \longrightarrow 4CoO(s){\cdot} + 12C(s) + 6CO_2\ (g) + 6C_5H_5N(g) + N_2(g) + H_2(g) \quad (3b)$$

$$4\ CoO(s) + 12C(s) + 2O_2{}^*(g) \longrightarrow 4Co^0\ (s) + 6C(s) + 8CO(s) \quad (3c)$$

$$4Co^0(s) + 2O_2{}^*(g) \longrightarrow 4CoO\ (s) \quad (3d)$$

*Residual O_2 in the N_2 purge gas.

3.3.2.4. Nickel compound. The TG–DSC curves of the compound are shown in Fig. 2d*. The first mass loss between 115 and 190 °C, corresponding to an endothermic peak at 170 °C is attributed to dehydration with loss of 4 H_2O ($\Delta m_{calcd.}$ = 19.22% (Eq. (4a)); Δm_{TG} = 19.38%).

The anhydrous compound is stable up to 295 °C and above this temperature the mass losses occur in two consecutive steps, being the first a fast process and the second a slow one. The first step between 295 and 400 °C corresponding to endothermic peaks at 332 °C and 368 °C suggesting overlapping steps, with mass loss of 49.26% ($\Delta m_{calcd.}$ = 51.25% (Eq. (13)) is attributed to thermal decomposition, with release of CO_2, C_5H_5N, (both identified by EGA), N_2 and H_2 (not detectable in IR). The second step between 400 and 890 °C, corresponding to a small (480 °C) and an indicium (640 °C) of endothermic peaks in the DSC curve, is attributed to the oxidation-reduction reaction between the nickel oxide and the carbonized material leading to the formation of Ni° and CO ($\Delta m_{calcd.}$ = 14.94% (Eq. (4c)), Δm_{TG} = 14.51%). The total mass loss up to 890 °C also suggest the formation of a mixture of Ni° and carbonaceous residue, in no simple stoichiometric relation ($\Delta m_{calcd.}$ Ni° = 84.34%, $\Delta m_{calcd.}$ Ni + C = 81.68%, Δm_{TG} = 83.42%), as confirmed by XRD and visual inspection. The small mass gain (Δm_{TG} = 1.27%) above 890 °C is attributed to the partial oxidation of the Ni° in the mixture to NiO [14,15].

$$Ni(IN)_2{\cdot}4H_2O(s) \longrightarrow Ni(IN)_2(s) + 4\,H_2O(g) \quad (4a)$$

$$4Ni(IN)_2(s) \longrightarrow 4NiO(s) + 12\,C(s) + 6\,CO_2(g) + 6\,C_5H_5N(g) + N_2(g) + H_2(g) \quad (4b)$$

$$4NiO(s) + 12C(s) + 2O_2(g)^* \rightarrow 4Ni^\circ(s) + 4C(s) + 8CO(g) \quad (4c)$$

$$4Ni^0(s) + xO_2(g)^* \rightarrow (4 - 2x)Ni\ (s) + (2x)NiO(s) \quad (4d)$$

*Residual O_2 in the N_2 purge gas

3.3.2.5. Copper compound. The TG–DSC curves are shown in Fig. 2e*. The first mass loss between 80 and 160 °C, corresponding to an endothermic peak at 145 °C, is attributed to dehydration with loss of 3.5 H_2O ($\Delta m_{calcd.}$ = 17.22% (Eq. (5a)); Δm_{TG} = 17.68%).

The anhydrous compound is stable up to 255 °C and above this temperature the mass losses occur in two consecutive steps, being the first a fast process, followed by a slow one. The first step between 255 and 290 °C with loss of 51.24% ($\Delta m_{calcd.}$ = 51.82% (Eq. (5b))),

corresponding to an endothermic peak at 285 °C in the DSC curve, is attributed to thermal decomposition of the compound, with release of CO_2, C_5H_5N, (both identified by EGA), N_2 and H_2 (not detectable by IR).

The second step between 290 and 810 °C, without thermal event in the DSC curve, is attributed to the oxidation-reduction reaction between the CuO and the carbonized material leading to the formation of Cu^0 and CO ($\Delta m_{calcd.}$ = 13.22% (Eq. (5c)), Δm_{TG} = 12.93%). The total mass loss up to 810 °C agrees with the formation of a mixture of Cu^0 and carbonaceous residue, in no simple stoichiometric relation ($\Delta m_{calcd.}$ Cu^0 = 82.86%, $\Delta m_{calcd.}$ Cu^0 + C = 79.62%, Δm_{TG} = 81.61%). The mass gain ($\Delta m_{calcd.}$ = 2.16% (Eq. (5d)); Δm_{TG} = 1.53%) above 810 °C and up to 1000 °C is attributed to oxidation reaction of the Cu^0 to Cu_2O.

$$Cu(IN)_2{\cdot}3.5H_2O(s) \longrightarrow Cu(IN)_2(s) + 3.5\ H_2O(g) \quad (5a)$$

$$4\ Cu(IN)_2\ (s) \longrightarrow 4CuO(s) + 12C(s) + 6CO_2\ (g) + 6C_5H_5N(g) + N_2(g) + H_2(g) \quad (5b)$$

$$4\ CuO(s) + 12\ C(s) + 3/2O_2(g) \longrightarrow 4\ Cu^0\ (s) + 5C(s) + 7CO(g) \quad (5c)$$

$$4\ Cu^0\ (s) + 3/2\ O_2{}^*(g) \longrightarrow 2\ Cu_2O(s) \quad (5d)$$

*Residual O_2 in the N_2 purge gas

3.3.2.6. Zinc compound. The TG–DSC curves of the zinc compound are shown in Fig. 2f*. The first mass loss between 40 and 140 °C, without thermal event in the DSC curve is attributed to dehydration with loss of 0.5 H_2O ($\Delta m_{calcd.}$ = 2.83%; Δm_{TG} = 2.28%):

The anhydrous compound is stable up to 365 °C and above this temperature the mass losses occur in two consecutive steps. The first step between 365 and 658 °C occurs through a fast process with mass loss of 59.09% ($\Delta m_{calcd.}$ = 60.32% (Eq. (19)), corresponding to an endothermic peak at 445 °C, is attributed to thermal decomposition of the compound, with release of CO_2, C_5H_5N (both identified by EGA), N_2 and H_2 (not detectable by IR). The second step occurs slowly between 400 and 900 °C, associated with endothermic peaks at 760 °C and 845 °C, is attributed to the oxidation-reduction reaction between the ZnO and the carbonized material leading to the formation of Zn^0 and carbon monoxide ($\Delta m_{calcd.}$ Zn^0 = 17.58% (Eq. (6c)), Δm_{TG} = 18.53%). The last observed endothermic peak at 945 °C can be attributed to the slow evaporation of Zn^0 [14–17].

$$Zn(IN)_2{\cdot}0.5H_2O\ (s) \longrightarrow Zn(IN)_2\ (s) + 0.5H_2O\ (g) \quad (6a)$$

$$4\ Zn(IN)_2\ (s) \longrightarrow 4ZnO(s) + 12C(s) + 6CO_2\ (g) + 6C_5H_5N(g) + N_2(g) + H_2(g) \quad (6b)$$

$$4\ ZnO(s) + 12C(s) \longrightarrow 4Zn^0\ (s) + CO(g) \quad (6c)$$

The exothermic peaks at 255 °C (Mn), 275 °C (Fe), 260 °C (Co), 235 °C (Cu) and 240 °C (Zn), without mass loss in the TG curve is attributed to a phase transition, which was further investigated by means of X-ray diffractometry.

3.3.3. Evolved gas analysis (TG–FTIR)

The gaseous products evolved during the thermal decomposition of the compounds studied in this work, in both atmospheres, were monitored by FTIR and are presented in Table 2. In both atmospheres the same gaseous species are produced. However, in air atmosphere pyridine is detected in lower amounts, probably due to oxidation in the furnace and/or heated transfer line during the diffusion to FTIR gas cell. The water vapor was omitted in Table 2, but it was identified in all analyzed compounds due to the dehydration step in TG curve (except Zn), and due to oxidation of organic material from ligand. Even in oxidative conditions (air atmosphere) CO could be detected for Ni compound in sensible amounts, which is usual in EGA experiments [18,19]

FTIR spectra of the gaseous products evolved for manganese compound in nitrogen atmosphere was chosen as representative for the series of compounds. A contour map plot of absorbance versus time of analysis is shown in Fig. 3. The dashed red squares highlight the regions where characteristic absorptions for each of the gaseous species identified occur. Reference spectra [20] are also presented in Fig. 3 to facilitate comparison. Individual spectra of evolved gases in both atmospheres for each compound are available in supplementary material.

Table 2
Gaseous products evolved during thermal decomposition isonicotinate complexes in dynamic dry air and N_2 atmospheres.

Compounds	Atmosphere	
	Air	N_2
HIN*	CO_2	CO_2, Py
NaIN*	CO_2, Py**	CO_2, Py
$Mn(IN)_2{\cdot}3H_2O$	CO_2	CO_2, Py
$Fe(IN)_2{\cdot}3.5H_2O$	CO_2	CO, CO_2, Py
$Co(IN)_2{\cdot}4H_2O$	CO_2, Py**	CO, CO_2, Py
$Ni(IN)_2{\cdot}4H_2O$	CO, CO_2, Py**	CO, CO_2, Py
$Cu(IN)_2{\cdot}3.5H_2O$	CO_2, Py**	CO_2, Py
$Zn(IN)_2{\cdot}0.5H_2O$	CO_2, Py**	CO, CO_2, Py

* IN = Isonicotinate.
** trace amounts of pyridine.

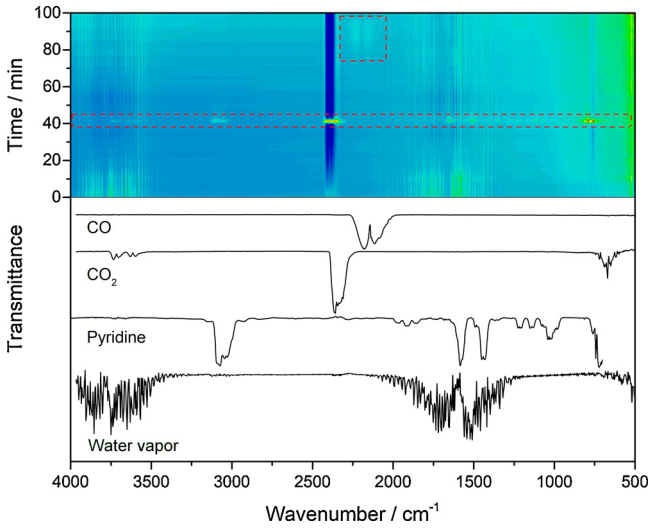

Fig. 3. Contour map of FTIR spectra collected during Mn compound thermal decomposition in N_2 atmosphere, and reference spectra for the identified evolved gaseous products.

3.4. Differential scanning calorimetry

The DSC curves of the compounds in dynamic dry air atmosphere are shown in Fig. 4. The endothermic peak at 125 °C (Mn), 147 °C (Fe), 154 °C (Co) 170 °C (Ni) and 142 °C (Cu) is attributed to dehydration and the calculated dehydration enthalpy was 159.3, 174.6, 268.6, 268.8 and 224.4 kJ mol^{-1}, respectively. The exothermic peak at 251 °C (Mn), 256 °C (Co), 244 °C (Cu) and 237 °C (Zn) is attributed to phase transition process and the enthalpy found was 13.7, 17.8, 18.8 and 17.0 kJ mol^{-1}, respectively.

Cyclic DSC experiments (heating/cooling/heating) in air atmosphere were performed with the compounds that presented exothermic events attributed to physical transformation. The cyclic curve for Manganese compound is shown in Fig. 5. It was concluded that this process is irreversible, once it was not possible to observe endothermic events in the DSC curve during the cooling cycle, and no exothermic event was observed on the second heating cycle. Besides that, to evaluate the long-term reversibility of this phenomenon, the aluminum

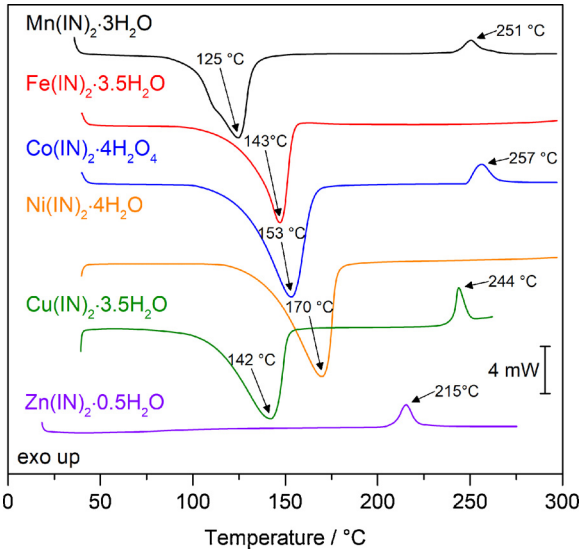

Fig. 4. DSC curves obtained in air atmosphere, showing the dehydration and phase transition temperatures.

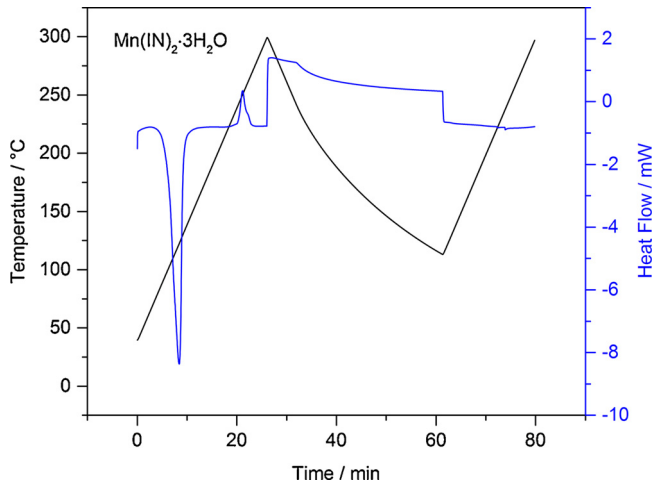

Fig. 5. Cyclic DSC (heating/cooling/heating) obtained for Mn compound, evidencing the irreversible character of the phase transition.

crucible used to perform the DSC experiment was allowed to rest for a few days in a desiccator, at ambient temperature and atmospheric pressure. A new DSC experiment was then performed, and no exothermic event was observed, confirming its irreversibility.

3.5. Infrared spectroscopy

The IR spectra of isonicotinic acid, sodium isonicotinate and its compounds with the bivalent metal ions considered in this work are shown in Fig. 6 and the assignments of the vibrational modes associated with the main bands are presented in Table 3. These assignments were based on literature data [4,21–24] and by comparison of the spectra of the compounds. For isonicotinic acid the ν(C = O) occurs in 1712 cm^{-1} and it is absent in the sodium salt and complexes' spectra. In the sodium salt spectrum two new bands (ν_{as}COO– and ν_{sym}COO–) appears in 1587 and 1409 cm^{-1} respectively, indicating the total deprotonation of the acid. This also confirms that the complexes do not present any protonated acid contamination.

The infrared spectra were also collected for the compounds heated at different temperatures, chosen according to events observed in the TG–DSC analysis. The FTIR spectra were recorded after dehydration and physical transformation of some compounds. The changes in

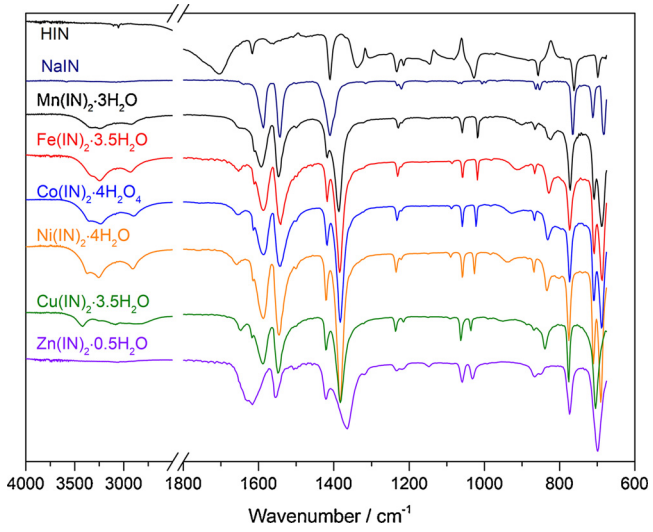

Fig. 6. FTIR spectra collected for isonicotinic acid, sodium isonicotinate and bivalent metal complexes.

intensity and wavenumbers of some absorption bands suggest that in both cases the compound's structures are altered, resulting in new crystalline arranges, intermolecular interactions and coordination mode.

For the sodium isonicotinate the asymmetric (ν_{as}COO–) and symmetric (ν_{sym}COO–) stretching frequencies are locate at 1542 cm^{-1} and 1410 cm^{-1}, respectively [24,25]. Analysis of the difference in the wavenumbers of $\nu_{as}COO^{-}$ and $\nu_{sym}COO^{-}$ bands ($\Delta\nu = \nu_{as} - \nu_{sym}$) are generally used as an indicative of coordination mode assumed by the carboxylate group in metal complexes [26,27]. The $\Delta\nu$ value observed the hydrated compounds is much larger (~204 cm^{-1}) then for sodium salt (178 cm^{-1}), although a close value was expected, because in this case the carboxylate acts generally as ion (uncoordinated) [5,6,13,28]. The hydrogen bonds formed with coordinated water molecules by this group causes a change in the charge distribution between the pyridine ring and the carboxylate group. This reflects in the vibration modes diverging from the observed for the sodium salt, making ambiguous the attribution of ionic carboxylate just by the analysis of symmetric and asymmetric stretching [27]. For the Zn compound, once it was obtained in an almost anhydrous state, the $\Delta\nu$ value (253 cm^{-1}) suggests that the carboxylate group also participates in the coordination with the metal in a unidentate coordination mode, once it is much larger than the observed for the sodium salt and the other compounds [26].

According to the crystalline structure described in the literature for these compounds, in which the two ligands coordinates to one metal center through the pyridine nitrogen atom in a *trans* configuration, and four coordinated water molecules, resulting in an approximately octahedral geometry [5,29] the dehydration process was expected to cause such change. This is because the crystalline lattice is held by hydrogen bonds formed between the oxygen atoms from the carboxylate group and the hydrogen atoms from coordinated water molecules. Upon dehydration, the crystalline lattice must reorganize to produce a new set of intermolecular interactions, which would affect mostly the carboxylate group [27]. This phenomenon reflects in the vibrational modes of this group in the FTIR spectra. In Fig. 7, the symmetric and asymmetric stretching of carboxylate group are slightly shifted to different wavenumbers in the spectra of the Co compound heated up to 200 °C when compared to the hydrated one. This could be related to a structure rearrangement and possibly the coordination of carboxylate oxygen to the metal ion upon dehydration, to maintain the coordination number of the metal [4]. However, just the IR data are not sufficient to undoubtedly assign the coordination of carboxylate upon dehydration.

After the physical transformation temperature (280 °C for Co

Table 3
Main infrared absorption bands assignments for sodium isonicotinate and metal complexes.

Assignment	NaIN	$Mn(IN)_2{\cdot}3H_2O$	$Fe(IN)_2{\cdot}3.5H_2O$	$Co(IN)_2{\cdot}4H_2O$	$Ni(IN)_2{\cdot}4H_2O$	$Cu(IN)_2{\cdot}3.5H_2O$	$Zn(IN)_2{\cdot}0.5H_2O$
β (O–H)	1639 w	1652 w	1655 w	1655 w	1657 w	1648 w	–
$\nu_{as}(COO^-)$	1587s (1546) [19]	1590 s	1587 s	1587 s	1587s (1583) [4]	1587 s	1616 s
$\nu(C-N)_{ar}$	1543 s	1547 s	1540 s	1542s	1545s (1542) [4]	1547 m	1553 m
$\nu(C-C)_{ar}$	Overlapped	1417 w	1417 w	1417 w	1421 w	1421 w	1421 w
$\nu_{sym}(COO^-)$	1409s (1411) [19]	1386 vs	1385 vs	1383 vs	1383 vs (1384) [4]	1383 vs	1363 vs
β(C–H)	1232 vw	1228 w	1230 w	1232 w	1234 w	1236 w	1234 vw
$\nu(C-C)_{ar}$	1221 w	1218 vw	1220 vw	1220 vw	1220 vw	1214 vw	1218 vw
β(C–H)	–	1059 w	1058 w	1058 w	1058 w	1061 w	1060 w
β(C–H)	–	1018 w	1018 w	1022 w	1025 w	1035 w	1031 w
γ(O–H)	–	900 w, br	912 w, br	925 w, br	939 w, br	952 w, br	–
γ(C–H)	862 w	866 w	866 w	866 w	867	867 w	865 w
γ(C–H)	853 w	–	–	–	–	–	850 w

ν: stretching; as: asymmetric; sym: symmetric; β: in-plane deformation; γ: out-of-plane deformation; ar: aromatic; vs: very strong; s: strong; m: medium; w: weak; vw: very weak; br: broad; –: absent.

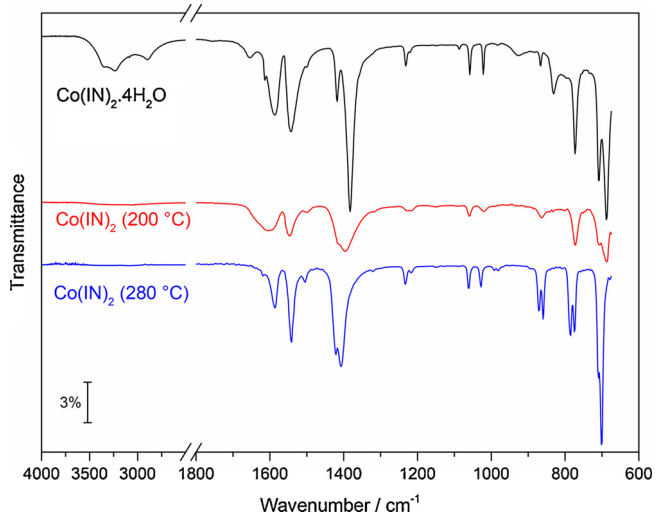

Fig. 7. Cobalt isonicotinate FTIR spectra obtained for hydrated, dehydrated (after heating to 200 °C) and phase transition temperature (after heating to 280 °C).

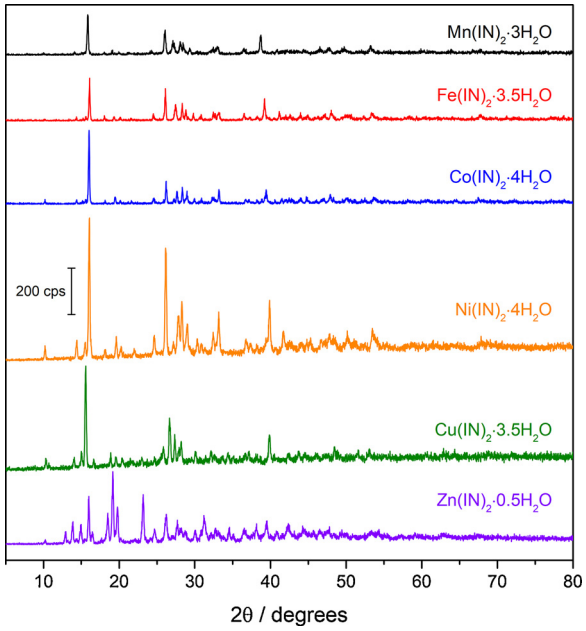

Fig. 8. PRXD patterns for the isonicotinate complexes.

compound) a different infrared absorption profile is observed, mainly in the range of 1000–675 cm^{-1}. This region is associated with the C=C ring stretching, so it can be suggested that the dehydration and physical transformation lead to a change in the charge distribution around the pyridine ring, which reflects in the shift of absorption bands. This observation provides further evidence that the exothermic event, observed in DSC curve, is attributed to a phase transition in the sample.

3.6. PXRD

The powder X-ray diffractograms in the Fig. 8 show that all the compounds were obtained in a crystalline phase. The great similarity of diffraction peaks in these diffractograms is evidence that these compounds form an isomorphous series.

Comparing the diffractograms with those previously reported in the literature for bivalent transition metals isonicotinate complexes [5], we can conclude that the compound synthesized in this work have the same stoichiometry and crystalline structure. Besides that, experimental mass loss and EA results agree with this conclusion.

Also, as previously discussed, the DSC curves of Mn, Co, Cu and Zn compounds show an exothermic event with no mass loss in the TG curve. To further investigate this physical process, the compounds were heated to a temperature above those indicated by the exothermic events in the DSC curve (280 °C for Mn, Co and Zn; 260 °C for Cu), and a diffractogram was acquired for each compound. The results are presented in Fig. 9. It can be seen a significative change in the diffraction pattern, with the disappearance of diffraction peaks and decrease of its intensity for all compounds. As expected, these results indicate a phase transition for the compounds, probably associated with the collapse/rearrange of the original crystal structure. However, these are qualitative observations that need further investigation, ideally by single crystal structural determination for the heated compounds.

4. Conclusions

This study aimed to synthesize some bivalent transition metal complexes with isonicotinate (4-pyridinecarboxylate) ligand and to investigate the thermal behavior under air and N_2 atmospheres, to determine the minimal formula, identify the evolved gases during thermal decomposition and pyrolysis, and to correlate structural characteristic with spectroscopic techniques.

From TG–DSC experiment and analytical results (EA and EDTA complexometry) it was possible to stablish a minimal formula for the compounds as $M(IN)_2{\cdot}nH_2O$ and to determine the purity of the synthesized compounds. Furthermore, from the TG–DSC curves it was possible to obtain previously unreported information about the thermal behavior (thermal stability, dehydration characteristics, profile and steps of thermal decomposition, intermediate compounds and final

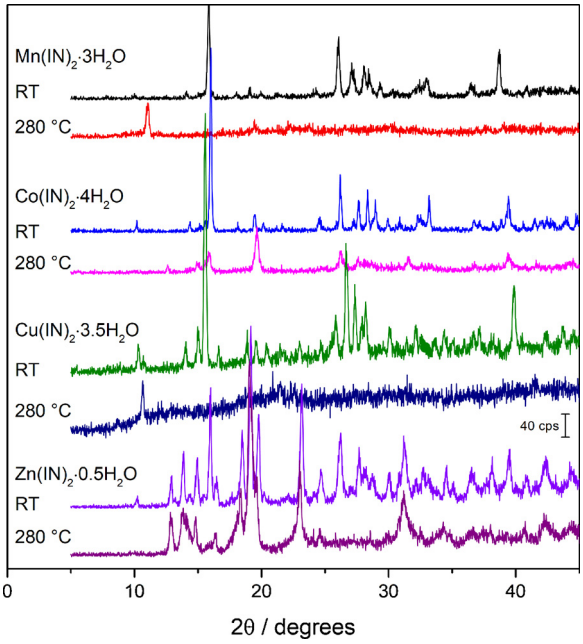

Fig. 9. PRXD patterns for Mn, Co, Cu and Zn complexes at room temperature (RT) and heated above the transition temperature.

residue) of these compounds in both conditions employed.

The results of TG–DSC and EGA show that the thermal stability and the initial thermal decomposition mechanism are little influenced by the conditions used (air or N_2), but it significantly influences the later stages, which suggests that the intermediate compounds formed are sensitive to conditions of analysis and / or the heat released in the oxidation of the volatiles contributes to accelerate the oxidation process of the organic matter.

The main gaseous products of thermal decomposition/pyrolysis of the compounds were identified as water vapor, CO, CO_2 and Pyridine, from which, together with the TG data, it was possible to suggest a thermal decomposition mechanism under N_2 atmosphere for the compounds.

Mn, Co, Cu and Zn compounds show a physical transformation process in DSC curves, which were further investigated through PRXD analysis that indicates a phase transition.

The infrared spectroscopic data was not capable of indicating the carboxylate coordination character. However, comparing the results with the ones previously reported in the literature we could conclude that the ligand coordinates through the pyridine nitrogen atom to the metal. For the Zn compound, the carboxylate group also participates in the coordination to the metal. Comparing the IR absorption profile of hydrated with dehydrated compounds it was possible to suggest that there is a probable change in the coordination mode of the ligand upon dehydration. This change needs to be further investigated, once it is not possible to ensure only with infrared spectroscopy data.

Acknowledgments

The authors thank FAPESP (Proc. 2017/14936-9), CNPq (Proc. 421469/2016-1) and CAPES foundations (Brazil) for financial support.

Appendix A. Supplementary data

Supplementary material related to this article can be found, in the online version, at doi:https://doi.org/10.1016/j.tca.2018.06.010.

References

[1] M.E. Chapman, P. Ayyappan, B.M. Foxman, G.T. Yee, W. Lin, Synthesis, X-ray structures, and magnetic properties of copper(II) pyridinecarboxylate coordination networks, Cryst. Growth Des. 1 (2001) 159–163, http://dx.doi.org/10.1021/cg005519l.
[2] J.Y. Lu, A.M. Babb, An extremely stable open-framework metal–organic polymer with expandable structure and selective adsorption capability, Chem. Commun. (2002) 1340–1341, http://dx.doi.org/10.1039/b200213b.
[3] M. Cortijo, S. Herrero, R. Jiménez-aparicio, J. Perles, J.L. Priego, Microwave-Assisted Synthesis of Tridimensional Nickel (II) Isonicotinate Complexes, (2011), pp. 9–10, http://dx.doi.org/10.1039/C0GC00800A.
[4] M. Cortijo, S. Herrero, R. Jiménez-Aparicio, J. Perles, J.L. Priego, M.J. Torralvo, J. Torroba, Hybrid polyfunctional systems based on nickel(II) isonicotinate, Eur. J. Inorg. Chem. (2013) 2580–2590, http://dx.doi.org/10.1002/ejic.201201461.
[5] Y. Chen, L. Li, J. Li, K. Ouyang, J. Yang, Ammonia capture and flexible transformation of M-2(INA) (M = Cu, Co, Ni, Cd) series materials, J. Hazard. Mater. 306 (2016) 340–347, http://dx.doi.org/10.1016/j.jhazmat.2015.12.046.
[6] B.K. Das, S.J. Bora, M. Chakrabortty, L. Kalita, R. Chakrabarty, R. Barman, Structural, thermal and spectroscopic properties of supramolecular coordination solids, J. Chem. Sci. 118 (2006) 487–494, http://dx.doi.org/10.1007/BF02703945.
[7] R. Xiong, S.R. Wilson, W. Lin, Bis(isonicotinato)iron(II): a rare, neutral three-dimensional iron coordination polymer, J. Chem. Soc. Dalton Trans. (1998) 4089–4090, http://dx.doi.org/10.1039/a806499g.
[8] Q. Wei, M. Nieuwenhuyzen, F. Meunier, C. Hardacre, S.L. James, Guest Sorption and Desorption in the Metal–Organic Framework [Co(INA) 2] (INA = Isonicotinate) – Evidence of Intermediate Phases During Desorption, (2004), pp. 1807–1811.
[9] E.E. Sileo, P.J. Morando, C.O. Della Vedova, M.A. Blesa, The thermal decomposition of copper(II) nicotinate and isonicotinate, Thermochim. Acta 138 (1989) 233–239, http://dx.doi.org/10.1016/0040-6031(89)87259-4.
[10] E.E. Sileo, P.J. Morando, M.A. Blesa, The different pathways of the thermal decomposition of metal nicotinates and isonicotinates, Thermochim. Acta 152 (1989) 299–306, http://dx.doi.org/10.1016/0040-6031(89)85399-7.
[11] C.N. de Oliveira, M. Ionashiro, C.A.F. Graner, Titulação Complexométrica de Zinco Cobre e Cobalto, Eclética Química 10 (1985) 7–10.
[12] A.L.C.S. Do Nascimento, F.J. Caires, D.J.C. Gomes, A.C. Gigante, M. Ionashiro, Thermal behaviour of nicotinic acid, sodium nicotinate and its compounds with some bivalent transition metal ions, Thermochim. Acta 575 (2014) 212–218, http://dx.doi.org/10.1016/j.tca.2013.10.014.
[13] M. Chakrabortty, J.N. Ganguli, S.J. Bora, B.K. Das, Thermal behaviour of metal (II) isonicotinate tetrahydrates, Indian J. Chem. 49 (2010) 876–881.
[14] A.C. Nascimento, F. Caires, T. Colman, M. Ionashiro, Thermal behavior of nicotinate of some bivalent transition metal ions in dry CO2 and N2 atmospheres, Braz. J. Therm. Anal. 4 (2015) 41, http://dx.doi.org/10.18362/bjta.v4.i4.232.
[15] F.J. Caires, D.J.C. Gomes, A.C. Gigante, L.S. Lima, C.T. Carvalho, M. Ionashiro, Thermal behavior of malonic acid, sodium malonate and its compounds with some bivalent transition metal ions in dynamic N2 and CO2 atmospheres, Brazilian J. Therm. Anal. 2 (2013) 12–16, http://dx.doi.org/10.18362/bjta.v2i1.4.
[16] R. Kernke, P. Hug, A. Reller, H.R. Oswald, Thermal reduction and reoxidation of spinel-type Cu1−xZnxAl2O4, J. Therm. Anal. 38 (1992) 611–618, http://dx.doi.org/10.1007/BF01979388.
[17] M.T. Šumar-Ristović, D.M. Minić, D. Poleti, Z. Miodragović, Đ. Miodragović, K.K. Anđelković, Thermal stability and degradation of Co(II), Cd(II), and Zn(II) complexes with N-benzyloxycarbonylglycinato ligand, J. Therm. Anal. Calorim. 102 (2010) 83–90, http://dx.doi.org/10.1007/s10973-010-0748-2.
[18] T. Ahamad, S.M. Alshehri, TG–FTIR– MS (evolved gas analysis) of bidi tobacco powder during combustion and pyrolysis, J. Hazard. Mater. 199–200 (2012) 200–208, http://dx.doi.org/10.1016/j.jhazmat.2011.10.090.
[19] Q. Li, C. Zhao, X. Chen, W. Wu, Y. Li, Comparison of Pulverized Coal Combustion in Air and in O2/CO2 Mixtures by Thermo-Gravimetric Analysis, (2009), http://dx.doi.org/10.1016/j.jaap.2008.10.018.
[20] S.E. Stein, "Infrared spectra" by NIST mass spec data center, in: P.J. Linstrom, W.G. Mallard (Eds.), NIST Chem. WebBook, NIST Stand. Ref. Database Number 69, National Institute of Standards and Technology, Gaithersburg, MD, 2018, , http://dx.doi.org/10.18434/T4D303.
[21] P. Koczoń, T. Hrynaszkiewicz, R. Świsłocka, M. Samsonowicz, W. Lewandowski, Spectroscopic (Raman, FT-IR, and NMR) study of alkaline metal nicotinates and isonicotinates, Vib. Spectrosc. 33 (2003) 215–222, http://dx.doi.org/10.1016/j.vibspec.2003.09.005.
[22] P. Koczoń, J. Piekut, M. Borawska, W. Lewandowski, Vibrational structure and antimicrobial activity of selected isonicotinates, potassium picolinate and nicotinate, J. Mol. Struct. 651–653 (2003) 651–656, http://dx.doi.org/10.1016/S0022-2860(03)00146-7.
[23] P. Koczoń, J.C. Dobrowolski, W. Lewandowski, A.P. Mazurek, Experimental and theoretical IR and Raman spectra of picolinic, nicotinic and isonicotinic acids, J. Mol. Struct. 655 (2003) 89–95, http://dx.doi.org/10.1016/S0022-2860(03)00247-3.
[24] R.M. Silverstein, F.X. Webster, Spectrometric Identification of Organic Compounds, 6th ed., Wiley, New York, 1998.
[25] K. Nakamoto, Infrared and Raman Spectra of Inorganic and Coordination Compounds, Part B, 5th ed., Wiley, New York, 1997.
[26] G. Deacon, R.J. Phillips, Relationships between the carbon-oxygen stretching frequencies of carboxylato complexes and the type of carboxylate coordination, Coord. Chem. Rev. 33 (1980) 227–250, http://dx.doi.org/10.1016/S0010-8545(00)

80455-5.
[27] V. Zeleňák, Z. Vargová, K. Györyová, Correlation of infrared spectra of zinc(II) carboxylates with their structures, Spectrochim. Acta Part A Mol. Biomol. Spectrosc. 66 (2007) 262–272, http://dx.doi.org/10.1016/j.saa.2006.02.050.
[28] L. Shen, J. Liu, Y. Xu, Synthesis and crystal structure of a cadmium complex with isonicotinate, J. Coord. Chem. 55 (2002) 123–127, http://dx.doi.org/10.1080/00958970211875.
[29] A. Anagnostopoulos, R.W. Matthews, R.A. Waltom, Studies on metal carboxylates. Part II. Cobalt(II) and nickel(II) complexes of certain pyridine carboxylic acids and pyridine-3-sulfonic acid: magnetic and spectral studies, Can. J. Chem. 50 (1972) 1307–1314.